A Model for Studying Drying at Hydrophobic Interfaces: Structural and Thermodynamic Properties†

Anders Wallqvist,‡ Emilio Gallicchio, and Ronald M. Levy*

Department of Chemistry, Rutgers University, Wright-Rieman Laboratories, 610 Taylor Road, Piscataway, New Jersey 08854-8087

Received: March 12, 2001; In Final Form: May 1, 2001

The structural and thermodynamic properties of a water droplet enclosed in a spherical cavity embedded in a hydrophobic material are studied. The structure of the interface between water and the hydrophobic material is analyzed as a function of cavity size, pressure, and the water−wall interaction potential. The propensity to form a density-enhanced (wet) or density-depleted (dry) interface is assessed by free-energy perturbation calculations. At high pressure, water wets the hydrophobic material, and at low pressure, the interface is dry. At ambient pressure, the specific equilibrium structure of the interface depends on the water−wall interaction potential. With a purely repulsive water−wall interaction potential, the water density at the interface is characteristic of a water−vapor interface (the dry state). The addition of dispersion attraction between water and the hydrophobic material causes notable structural changes; the width of the interface is reduced from approximately 4 Å to less than 1 Å, and the water droplet comes into contact with the wall. The water density at the wall, however, is depleted relative to the wet state. The results obtained in this work provide insights into the hydration properties of large hydrophobic molecular assemblies.

1. Introduction

Experimental and theoretical studies[1] have thoroughly characterized the structural and the thermodynamic properties of hydration of small hydrophobic solutes. A picture has emerged according to which water is able to efficiently reorganize around nonpolar solutes inducing only relatively small enthalpic and entropic losses. Solvent-induced hydrophobic interactions have been observed which lead to formation of solvent-separated pairs of small hydrophobic solutes at low solute concentrations and lead to the formation of stable hydrophobic assemblies at sufficiently high solute concentration.[2−18]

The properties of water at interfaces[19] or near large nonpolar structures, however, are still matter of investigation.[20,21] There is some evidence to indicate that simple extrapolation of the hydration properties from the small hydrophobic solute regime to the large hydrophobic solute regime is not appropriate.[22−24] The key difference lies in the reduced ability of water to efficiently reorganize around large impenetrable objects, and as a result, a large free-energy penalty is associated with such interfaces. Several liquid state theories predict, in fact, that at standard thermodynamic conditions water does not wet a nonpolar surface but rather a vapor layer separates water from the surface.[25,26] This conclusion is supported by surface force measurements between nonpolar plates in water that indicate the occurrence of a drying transition even at large (>10 nm) surface separations.[27,28] Explicit solvent computer simulations of water near hydrophobic surfaces or large hydrophobic solutes,[29−33] however, did not indicate a propensity of water toward drying at the interface. Lum et al.[26] have pointed out that a drying transition at a large plate separation is a kinetically frustrated process difficult to observe in explicit solvent simulations. Wallqvist and Berne[34] have shown that in a explicit solvent constant pressure simulation drying occurs between plates but at a separation less than two water diameters. The simulation results of Hummer and Garde[35] indicate that a vapor layer at most a few molecules wide (weak dewetting) occurs around large repulsive solute cavities because of the loss of water−water interaction energy in the area closest to the cavity. They suggest, however, that weak dewetting will be less pronounced when the attractive solute−water dispersion interactions are taken into account.

A better understanding of the hydration properties of large hydrophobic assemblies is important in many areas,[36] particularly in biological applications. The formation of micelles and phospho−lipid membranes and their mechanism of interaction with plasma and membrane proteins involve the hydration of large hydrophobic molecular assemblies.[37] The structure and properties of proteins in water is highly influenced by hydrophobic interactions between nonpolar residues.[22,38−40] Hydrophobic interaction also plays a key role in the mechanism of ligand binding to proteins.[41−43]

In this paper, we investigate by computer simulations a simple model that elucidates some aspects of the properties of water at the interface between the liquid and a hydrophobic surface. The model consists of a water droplet enclosed in a spherical cavity embedded in a hydrophobic continuum. Because the water phase in our model is finite, the simulation does not require the adoption of periodic boundary conditions or the inclusion of long-range electrostatic corrections. The structure of the interface between the water droplet and the wall of the cavity is analyzed as a function of cavity radius. Free-energy perturbation calculations are carried out by varying directly the cavity radius to measure quantitatively the stability of the interface. By varying the cavity radius, wetting/drying transitions are

† Part of the special issue "Bruce Berne Festschrift".

* To whom correspondence should be addressed.

‡ Current address: Frederick Cancer Research and Development Center, National Cancer Institute, Science Applications International Corporation, Frederick, MD 21702-1201.

10.1021/jp010945i CCC: $20.00
Published on Web 06/13/2001

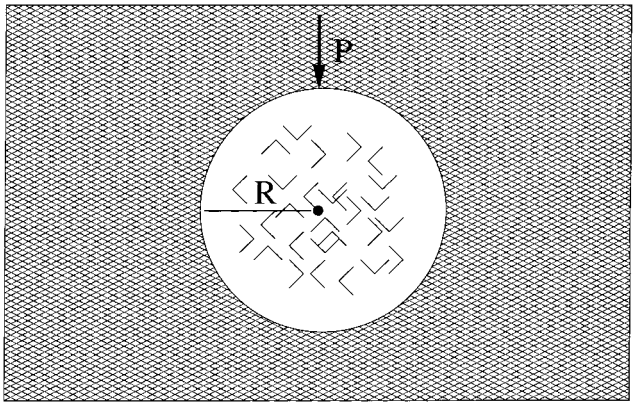

Figure 1. Schematic representation of the system studied. The shaded area represents the continuum hydrophobic medium.

induced explicitly so as to overcome the kinetic barriers that may have affected the results of previous simulations. The predictions of the model have been extensively correlated with variations of the model parameters, and the convergence behavior with respect to system size has been analyzed.

2. Description of the Model

The model studied is shown schematically in Figure 1. It consists of a spherical cavity containing N water molecules enclosed in an hydrophobic continuous material. The volume of the hydrophobic medium is macroscopically large but finite. The hydrophobic medium is impenetrable to water; it is considered composed of particles that do not interact with each other but that interact with the water molecules in the cavity. The density of the hydrophobic medium is uniform outside the cavity. Under these assumptions (see Appendix A), the canonical configurational partition function of the system at the cavity radius R is

$$Q(R) = \int \mathrm{d}^{\mathrm{N}}\mathbf{r}\, \exp\{-[U_{\mathrm{ww}}(\{\mathbf{r}\}) + U_{\mathrm{wh}}(\{\mathbf{r}\};R) + PV(R)]/kT\} \quad (1)$$

where $\{\mathbf{r}\}$ are the coordinates of the N water molecules, U_{ww} is the water−water potential energy, U_{wh} is the average water−hydrophobic medium potential energy, $V(R) = 4\pi R^3/3$ is the volume of the cavity, and P is the pressure exerted by the hydrophobic medium on the cavity. The Helmoltz free energy from eq 1 is

$$A(R) = -kT \ln Q(R) = F(R) + PV(R) \quad (2)$$

where $F(R)$, the free energy of the water droplet, is defined as

$$\exp(-F(R)/kT) = \int \mathrm{d}^{\mathrm{N}}\mathbf{r}\, \exp\{-[U_{\mathrm{ww}}(\{\mathbf{r}\}) + U_{\mathrm{wh}}(\{\mathbf{r}\};R)]/kT\} \quad (3)$$

When not constrained, the cavity radius equilibrates to a value R_{eq} that can be varied by varying the pressure P exerted by the hydrophobic medium. As shown in Appendix B, in the thermodynamic limit ($N \rightarrow \infty$), R_{eq} is the minimum of $A(R)$ and $A(R_{\mathrm{eq}})$ equals the Gibbs free energy $G(P)$ of the water droplet (considering the hydrophobic continuum as part of the environment) at the pressure P. The model therefore allows us to infer the thermodynamics of the water droplet in the cavity at constant pressure. In principle, the same result could be achieved by considering the Gibbs ensemble for the water droplet in the cavity; however, because wetting/drying transitions are known to be kinetically frustrated processes,[44] in practice, there is no assurance that the cavity radius will equilibrate to the true free-energy minimum at the given pressure during the simulation time.

The size of the cavity at equilibrium is determined by the balance between opposing thermodynamic forces. The exclusion volume interactions between water molecules and between the water molecules and the hydrophobic wall prevent the cavity from collapsing and favor large cavity radii. The attractive interactions between water molecules, on the other hand, favor compact cluster geometries, and the external pressure tends to contract the cavity and the water cluster.

The goal is to determine the structure of the interface between the water cluster and the hydrophobic wall at equilibrium. We consider the following general characteristics of the interface: (i) the presence of a vapor layer separating the water droplet surface from the wall or the absence of a vapor layer when the water droplet surface is in direct contact with the wall and (ii) the average water density in proximity to the wall which can be either smaller (density depleted) or larger (density enhanced) than the bulk density. An interface with a vapor layer separating the water droplet from the wall is density depleted. A density enhanced state is observed under some conditions when the water droplet surface is in contact with the wall. In the literature, the density enhanced interface is often referred to as being wet, whereas the density depleted interface is often referred to as being dry.[26] In the following, we will refer to wetting and drying transitions in this model with the understanding that these transitions, which occur on a microscopic scale, cannot be considered true phase transitions. Similarly, we will refer to the low water density region at the interface between the water droplet and the wall as the vapor layer although it is not a true macroscopic vapor phase.

It is difficult to predict using general criteria whether a vapor layer is likely to form under some given thermodynamic conditions. The "contact state", for which the water droplet is in direct contact with the wall, occupies less volume, is favored by the volume work, and does not involve the formation of a vapor phase which has a larger chemical potential than the liquid for the thermodynamic conditions we are considering. The formation of a vapor layer, however, is expected to be favored by the concomitant reduction of water surface tension because the wall−water surface tension, due to the energetic and entropic losses suffered by the water molecules in contact with the wall, is likely to be larger than the water−vapor and vapor−wall surface tensions at the given thermodynamic conditions.

The structure of the interface can be analyzed by calculating, using computer simulations, the water density profile at the interface. For a wet state, the water density profile shows a peak greater than that of the bulk density which is sharp and the density rapidly decays to zero as the wall is approached. For a dry state, the water density profile decays slowly and monotonically as for a water cluster in equilibrium with the surrounding vapor. Under some conditions, we have observed a contact state which lacks the density enhancement that is the signature of a wet state but also lacks the vapor layer characteristic of a dry state.

This model is appropriate to study the structure of water near concave nonpolar regions on the surface of large molecules such as proteins. The extrapolation to the $N \rightarrow \infty$ limit, at which the curvature of the cavity is zero, allows the model to be applied to the study of the structure of water near planar hydrophobic walls. To this end, we have also introduced (see below) a wall−water interaction potential to minimize the effect of the curvature of the cavity on the structure of the interfacial water layer. The

intensive thermodynamic quantities calculated are reasonably converged with respect to system size.

3. Computational Procedure

3.1. Model Interactions. For water−water interactions, we employ the SPC/E interaction model,[45] a fixed-charge model with rigid interaction sites carrying effective charges on an oxygen and hydrogen-like sites with a single Lennard-Jones center at the oxygen site. This model gives good liquid water properties for a range of physical conditions.

The interaction potential between a water molecule and the hydrophobic medium has been derived assuming the medium is composed of uniformly distributed methane molecules. The number density of the methane molecules is denoted by ρ. The methane−water pair potential is taken as the Lennard-Jones 6-12 potential. The analytical expression for the average hydrocarbon medium−water interaction potential $u(r;R)$ is obtained by integrating the Lennard-Jones pair potential over the volume of the hydrocarbon medium:

$$u(r;R) = \rho \int_{|\mathbf{r}'|>R} 4\epsilon\left[\left(\frac{\sigma}{|\mathbf{r}'-\mathbf{r}|}\right)^{12} - \left(\frac{\sigma}{|\mathbf{r}'-\mathbf{r}|}\right)^{6}\right] \mathrm{d}^3\mathbf{r}'$$

$$= 2\pi\epsilon\rho\sigma^3\left\{\frac{2\sigma^9}{45(R-r)^9} + \frac{\sigma^9}{20r(R-r)^8} - \frac{\sigma^3}{3(R-r)^3} - \frac{\sigma^3}{2r(R-r)^2} + \frac{2\sigma^9}{45(R+r)^9} - \frac{\sigma^9}{20r(R+r)^8} + \frac{\sigma^3}{3(R+r)^3} + \frac{\sigma^3}{2r(R+r)^2}\right\} \quad (4)$$

where $\mathbf{r}$ is the position of the water oxygen from the center of the cavity and R is the radius of the spherical cavity. The ϵ and σ Lennard-Jones parameters are set as to mimic the water−methane interaction; their values are taken as 3.4475 Å and 0.8927 kJ/mol, respectively.[13] Two states of the hydrophobic medium have been investigated: a high density state, $\rho = 0.0233$ Å^{-3} ($\rho^* = \sigma^3\rho = 0.955$), and a low density state, $\rho = 0.008$ Å^{-3} ($\rho^* = 0.328$).

A modified version of the potential in eq 4 was also used in order to study the effect of the shape of the cavity. A water molecule in a small spherical cavity interacts strongly with the hydrophobic medium because it is surrounded by it from any direction. In contrast, a molecule interacts strongly with a planar hydrophobic wall at a smaller distance from the wall. This behavior can be approximately obtained in a spherical geometry by modifying the potential in eq 4 in such a way that the wall will appear locally planar. This is achieved using eq 4 by letting r and R go to infinity while keeping the wall−water distance $R - r$ constant, obtaining

$$u_\infty(r;R) = 2\pi\epsilon\rho\sigma^3\left\{\frac{2\sigma^9}{45(R-r)^9} - \frac{\sigma^3}{3(R-r)^3}\right\} \quad (5)$$

with the symbols given as above. Using this potential, a molecule at a distance $R - r$ from the spherical wall will, effectively, interact with a planar wall at a distance $R - r$ tangent to the closest point of the wall. The 9-3 potential form (eq 5) has been used before to describe the interaction of a water molecule with a planar nonpolar wall.[31,46,47] The potentials from eqs 4 and 5 are shown in Figure 2 for typical values of R and for $\rho = 0.0233$ Å^{-3}. The $u_\infty(r;R)$ potential is not as strongly attractive as $u(r;R)$ especially for small R. The intensity and shape of the $u(r;R)$ potential changes with R as it approaches

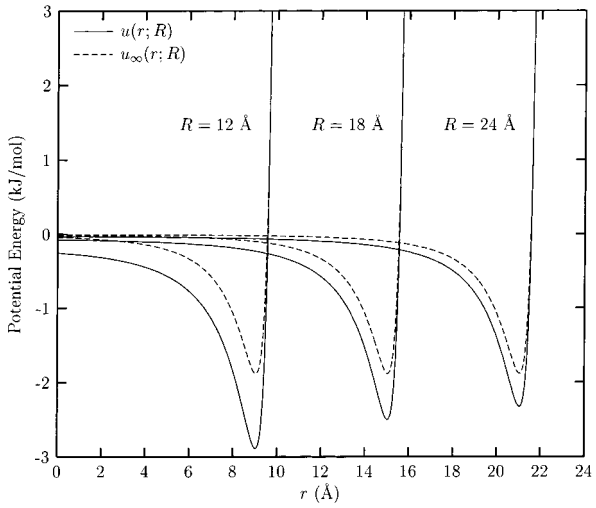

Figure 2. Water−hydrocarbon medium interaction potentials $u(r;R)$ (eq 4) and $u_\infty(r;R)$ (eq 5) as a function of the radial distance from the center of the cavity of the oxygen atom of a water molecule. The potentials are given for $R = 12$, 18, and 24 Å and for $\rho = 0.0233$ Å^{-3}.

$u_\infty(r;R)$ for large R. The potentials at the smaller methane density $\rho = 0.008$ Å^{-3} are about three times less intense than those shown in Figure 2. Notice that the distance of closest approach of an oxygen nucleus to the wall is about 2 Å less than R.

We have also considered pure repulsive interaction potentials between the wall and the water molecules. The repulsive potentials are obtained from the total potentials from eqs 4 and 5 by removing the attractive part as defined for the WCA liquid state theory[48]:

$$u^{\mathrm{rep}}(r) = \begin{cases} 0 & r < r_{\min} \\ u(r) - u(r_{\min}) & r \geq r_{\min} \end{cases} \quad (6)$$

where $r_{\min}$ denotes the location of the minimum of the total potential $u(r)$.

3.2. Free-Energy Calculations. We have performed free-energy perturbation calculations to identify the cavity size corresponding to a minimum of the Helmholtz free energy $A(R)$ of the system. The minimum is identified by calculating the free energy $F(R)$ of the water droplet at various cavity radii and by locating the minimum of $A = F(R) + PV(R)$, where $V(R)$ is the volume of the cavity and P is the pressure exerted by the hydrophobic medium. It is necessary to perform the computationally expensive evaluation of $F(R)$ only once to obtain $A(R)$ at any pressure.

The free-energy perturbation method (FEP) is used to calculate the free-energy difference ΔF_{ij} between two states i and j

$$\Delta F_{ji} = F(j) - F(i) = -kT \ln\langle \mathrm{e}^{-[U(j) - U(i)]/kT}\rangle_i \quad (7)$$

where k is Boltzmann's constant and the brackets indicate an ensemble average at the reference state i. Here $U(i)$ represents the total potential energy of the current configuration of the system in state i. Canonical ensemble averages at fixed cavity radius were obtained by integrating the equations of motion using the Rattle version[49] of the velocity Verlet algorithm[50] in order to constrain the internal bond lengths as well as the bond angle of the water molecules. The time step was set to 2.0 fs. The temperature was maintained constant by periodically rescaling the velocities. Both the translational and rotational temperatures were monitored so as to avoid a temperature imbalance between these degrees of freedom. All interactions

were spherically truncated at 9.3 Å. A set of simulations with different potentials and for different system sizes were carried out varying the R parameter in eqs 4 and 5. In this case, in eq 7, $U(i)$ is the potential energy of the system when $R = R_i$ and $U(j) - U(i) = U_{wh}(R_j) - U_{wh}(R_i)$ where $U_{wh}(R)$ is the total water−hydrophobic medium potential energy. The value of $\Delta F(R_i) = F(R_i) - F(R_0)$ for the state at $R = R_i$ with respect to the reference state at $R = R_0$ is obtained by summing over the intermediate free-energy changes

$$\Delta F(R_i) = \sum_{j=0}^{i} \Delta F_{j+1j} \tag{8}$$

where ΔF_{j+1j} is given by eq 7 setting $i = j + 1$. The value of $\Delta A(R_i)$ is obtained by adding the pressure−volume work $P\Delta V(R_i) = PV(R_i) - PV(R_0)$ to $\Delta F(R_i)$

$$\Delta A(R_i) = \Delta F(R_i) + P\Delta V(R_i) \tag{9}$$

where $V(R) = 4\pi R^3/3$.

Free-energy perturbation calculations were also carried out for the process of removing the attractive component of the total potential $u(r;R)$ at a fixed R value. This transformation was accomplished by introducing a perturbation parameter λ

$$u(r;R,\lambda) = (1 - \lambda)u(r;R) + \lambda u^{rep}(r;R) \tag{10}$$

in such a way that $u(r;R)$ is converted to $u^{rep}(r;R)$ as λ goes from 0 to 1.

Thermodynamic averages were calculated for each state by block averaging five simulations of 5.0 picoseconds each. The statistical uncertainties of the calculated free energies are estimated as twice the standard deviation obtained from block averaging. The resulting errors in the free energies are less than 1% and are omitted in the discussion below. The free-energy profiles as a function of cavity radius were obtained with a resolution of 0.02 Å (300 FEP windows for the transformation from $R = 18$ to $R = 24$ Å). A total of 100 FEP windows were employed to evaluate the free-energy change for the process of removing the attractive part of the total wall−water potential.

4. Results and Discussion

4.1. Structure of Water at the Interface. A state in which a vapor layer separates the water droplet from the cavity wall (separated state) is characterized by a water density profile at the interface similar to that of the water−vapor interface. We have therefore obtained data for a water cluster in a vacuum [$u(r;R) = 0$] for comparison purposes. The oxygen density within the bulk region of the cluster is found to be uniform. The water model studied here does not exhibit strong structural ordering at the interface; the water density smoothly drops off to zero in a layer 4 Å thick, as measured by the range of distances in which the density decreases from 90 to 10% of the bulk value. The water density profile at the interface varies somewhat with the size of the cluster. The location of the interface, as measured by the distance at which the density drops to half of the bulk value, is at 18.325 Å for $N = 905$ and 8.975 Å for $N = 113$, corresponding to curvatures of 0.0546 Å^{-1} and 0.1114 Å^{-1}, respectively. Compared to a previous study of a planar interface[33] the shape of the larger sized-cluster vacuum interface is similar despite differences in the underlying water model.

The structure of the water cluster enclosed in the cavity surrounded by the hydrophobic medium varies significantly depending on the radius of the cavity R. Figure 3 shows the

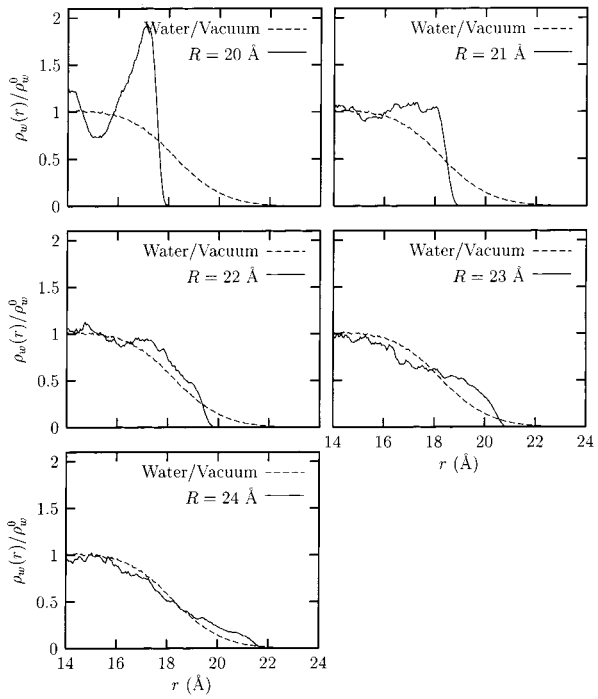

Figure 3. The water density profile obtained using the attractive water−wall interaction potential $u(r;R)$ (eq 4) and $N = 905$ as a function of the distance from the center of the cavity. The water density profile is shown for $R = 20-24$ Å. Note that the distance of closest approach of an oxygen nucleus to the wall is approximately 2 Å less than R (see Figure 2).The density is expressed as the ratio between the water density $\rho_w(r)$ and the density of liquid water ρ_w^0 at standard conditions ($T =$ 298 K and $P = 1$ atm).

calculated water density profiles at the interface for $N = 905$ for various values of R using the attractive wall−water potential of eq 4. For small values of R, the cavity compresses the water droplet and a wet interface is formed as indicated by the density maximum and the steep density reduction in proximity to the wall (see the density distribution at $R = 20$ Å).

As the size of the cavity is increased (see the density distribution at $R = 21$ Å), the density peak at the interface is significantly reduced signifying the incipient drying of the cavity wall. The water density, however, is roughly constant up to the wall where it drops to zero in less than 1 Å, a range of distances as small as in the wet state. At this stage, the water droplet is still considered to be in contact with the cavity wall. This state is intermediate between wet and dry and we refer to it as a "contact" state.

For larger values of the cavity radius R (see the density distributions at $R = 22$ and 23 Å), the density profile assumes a shape similar to that of the water−vacuum interface and is clearly consistent with a dry state. At $R = 24$ Å, the width of the interface is as wide as that of the water−vacuum interface. At this point, the interface is considered to contain a fully formed vapor layer separating the water droplet from the cavity wall. The water−vacuum interface, however, is not exactly reproduced. Instead, some water molecules become adsorbed onto the wall. This is indicated by the bump around 21 Å of the density distribution function for $R = 24$ Å relative to the water−vacuum reference density distribution shown in Figure 3. Moving the wall even further out causes the adsorbed water molecules to be dragged with it. A certain number of water molecules appear to be always associated with the hydrocarbon medium regardless of cavity radius when the interaction potential includes the attractive term. This phenomenon has been observed also for the $u_\infty(r;R)$ potential (eq 5) that has a shallower

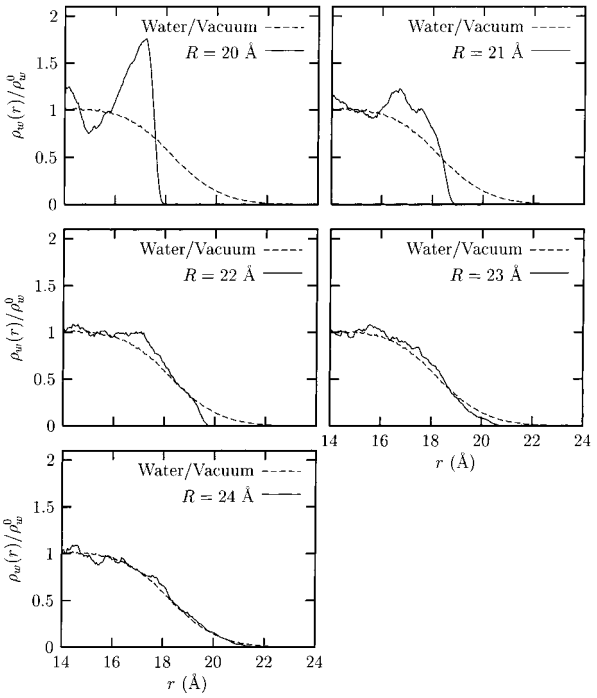

Figure 4. water density profile obtained using the repulsive water−wall interaction potential $u^{rep}(r;R)$ (eq 6) and $N = 905$ as a function of the distance from the center of the cavity. See the caption of Figure 3 for other definitions.

energy minimum at the wall (Figure 2) and by decreasing the methane density to $\rho = 0.008$.

A similar pattern is observed with the repulsive wall−water interaction potential (eq 6; see Figure 4). As before we observe an enhancement of the water density at the wall that consequently subsides as R is increased. For $R = 24$, however, the water−vacuum density distribution is almost exactly recovered. Under these conditions, there are no water molecules adsorbed on the surface of the wall.

4.2. Equilibrium States. Figure 5 shows the Helmoltz free energy of the system $A(R) = F(R) + PV(R)$ as a function of cavity radius for some representative values of the hydrophobic medium pressure. At the minimum in each curve, $\Delta A(R_{min}) = \Delta G(P(R_{min}))$, see Appendix B.

The free-energy minimum for the attractive water−hydrophobic medium potential at $P = 1$ atm occurs at $R = 21.2$ Å which corresponds to the contact state that lacks the density enhancement (see the $R = 21$ Å density profile shown in Figure 3). The location of the minimum of $\Delta A(R)$ moves to smaller radii as the pressure is increased. At $P = 1000$ atm, the minimum is close to $R = 20$ Å which corresponds to a wet interface.

The minimum of the free energy for the attractive potential is rather insensitive to applied pressure. The location of the minimum of $\Delta A(R)$ for the repulsive potential, instead, occurring beyond $R = 24$ Å at 1 atm, moves rapidly to lower values of R as the pressure in increased. Figure 6 shows the position of the Helmoltz free-energy (or Gibbs free-energy) minimum for the repulsive potential as a function of pressure. At 1 atm, the minimum is beyond the range of cavity radii examined, and at 10 atm, the minimum is around $R = 24$ Å. Statistical uncertainties in the calculations make it difficult to locate the minimum with high accuracy in this regime; it is nevertheless clear that at ambient and moderate pressures the repulsive cavity wall is dry and that at low pressures the size of the vapor layer is large (≥4 Å). As the pressure is increased, the value of R at

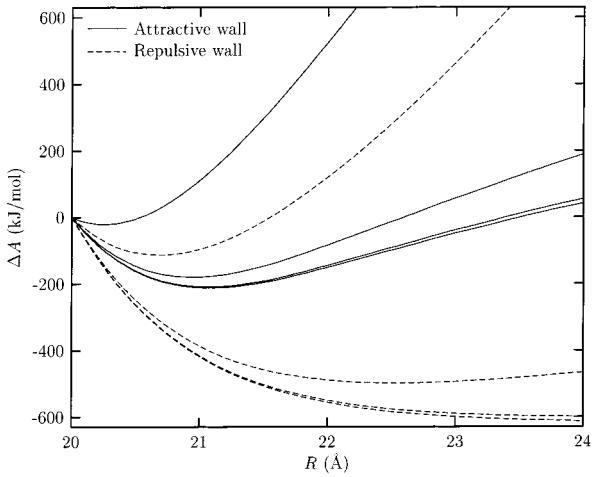

Figure 5. Helmoltz free energy as a function of the cavity radius R obtained using the attractive $u(r;R)$ and repulsive $u^{rep}(r;R)$ water−wall potentials at $N = 905$ and $\rho = 0.0233$ Å^{-3} at the pressures $P = 1$, 10, 100, and 1000 atm (the larger the pressure the higher the position of the corresponding free-energy curve). The minimum of the free-energy shift to lower values of R as the external pressure increases. The zero of the free energy is arbitrarily assigned to the free energy corresponding to the smallest R studied at the given pressure. At the minimum in each curve, $\Delta A(R_{min}) = \Delta G(P(R_{min}))$, see Appendix B.

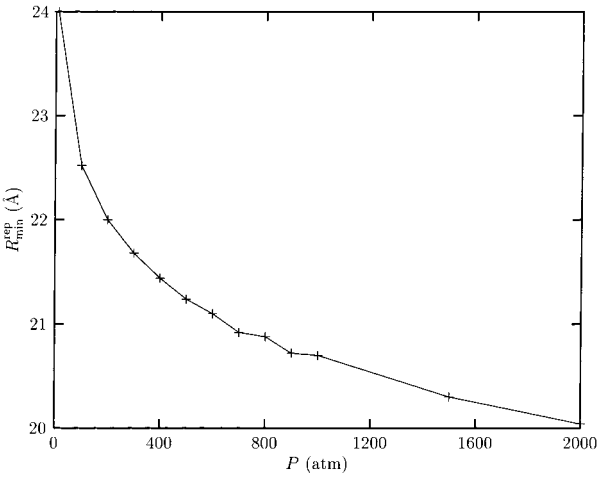

Figure 6. Cavity radius at the minimum of the Helmoltz free energy (or, equivalently, of the Gibbs free energy) as a function of applied pressure for the repulsive water−wall interaction $u^{rep}(r;R)$, $N = 905$, and $\rho = 0.0233$ Å^{-3}.

the free-energy minimum decreases, and eventually, a wet state is formed even with the purely repulsive potential. This occurs at roughly 1000 atm.

The presence of the dispersion attraction causes large changes of the equilibrium structure of the interface at ambient conditions. Figure 7 compares the computed water density distributions for the attractive potential at $R = 21$ Å and for the repulsive potential at $R = 24$ Å corresponding to the equilibrium states at 10 atm with and without the attractive water−wall interaction term. The equilibrium with the attractive potential is the "contact" state described in the previous section; the water droplet is in contact with the wall, and the density at the wall is reduced with respect to the wet state. The equilibrium state with the repulsive potential is the dry state which corresponds to a much wider interface (≥4 Å) characteristic of a water−vapor interface.

4.3. Drying Work and Surface Tension. At ambient pressure, the formation of a vapor layer between the water

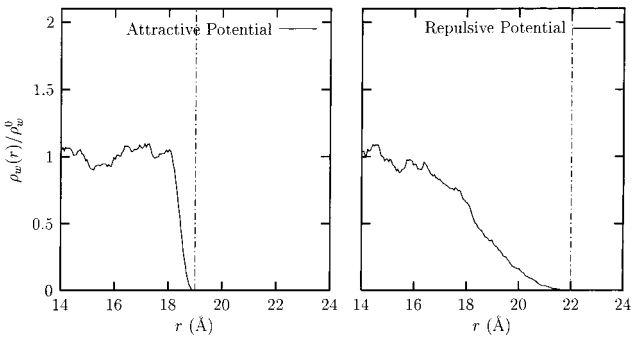

Figure 7. Water density profiles of the equilibrium states obtained using the attractive ($R = 21$ Å) and repulsive ($R = 24$ Å) water−wall interaction potential at 10 atm pressure and 298 K. The dash−dotted vertical lines indicate the approximate distance of closest approach between the water molecules and the wall.

droplet surface and the wall is disfavored when the attractive term is included in the water−hydrophobic medium potential. In this section, we estimate the tendency toward the contact state by calculating the work required to form the separated dry state obtained with the repulsive water−hydrophobic medium potential at ambient pressure. Simply taking the difference of the attractive water−hydrophobic medium potential Helmoltz free energies, calculated at the cavity radii corresponding to the two states, would not be representative because at large cavity radii a pure separated dry state is not found as water molecules are adsorbed onto the cavity wall. For this purpose, we define, therefore, the separated state as the equilibrium state obtained with the repulsive wall−water interaction under 10 atm pressure and the contact state as the equilibrium state corresponding to the attractive potential under 10 atm pressure. The equilibrium states correspond to the values of the cavity radii at the minimum of $A(R)$, $R_{min} = 21.1$ Å and $R_{min}^{rep} = 24.0$ Å, for, respectively, the total and repulsive wall−water potentials. The 10 atm pressure was chosen because it is the smallest pressure for which a minimum of $A(R)$ with the repulsive water−hydrophobic medium potential was identified. We then performed the same procedure without the attractive water−hydrophobic medium potential energy term to estimate the tendency of the system to form a dry state with the repulsive water-hydrophobic medium potential (ΔA_2 in Figure 8).

Referring to the thermodynamic cycle shown in Figure 8 the work, ΔA_s, required to form the dry state in the presence of an attractive potential is given by

$$\Delta A_s = \Delta A_1 + \Delta A_2 + \Delta A_3$$
$$= \Delta A[u(r;R_{min}) \rightarrow u^{rep}(r;R_{min})] + \Delta A[u^{rep}(r;R_{min}) \rightarrow u^{rep}(r;R_{min}^{rep})] + \Delta A^{irr}[u^{rep}(r;R_{min}^{rep}) \rightarrow u(r;R_{min}^{rep})] \quad (11)$$

where ΔA^{irr} indicates the free-energy change for the irreversible process of adding the wall−water attraction to the separated state without allowing the water cluster to relax. (The corresponding reversible process would instead generate the state we started from, yielding $\Delta A_s = 0$.) The quantity $\Delta A^{irr}[u^{rep}(r;R_{min}^{rep}) \rightarrow u(r;R_{min}^{rep})]$ is defined as the average of the attractive part of the water−wall interaction at the state corresponding to the repulsive water wall interaction

$$\Delta A^{irr}[u^{rep}(r;R_{min}^{rep}) \rightarrow u(r;R_{min}^{rep})] = \langle u(r;R_{min}^{rep}) - u^{rep}(r;R_{min}^{rep})\rangle_{rep} \quad (12)$$

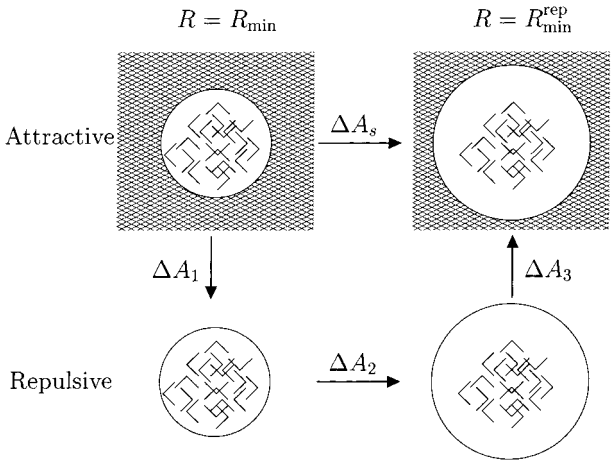

Figure 8. Thermodynamic cycle used to measure the propensity of water to form the contact state in the presence of the attractive water−wall potential. The states on the left correspond to the cavity radius R_{min}, and the states on the right correspond to the cavity radius R_{min}^{rep} defined as the radii for which $\Delta A(R)$ is a minimum for, respectively, the total wall−water potential and the repulsive wall−water potential under 10 atm external pressure. The states in the upper portion of the diagram correspond to the total water−wall interaction potential and the ones in the lower portion to the repulsive water−wall interaction potential. The state in the upper-right corner is a meta-stable separated state with the attractive wall−water potential.

TABLE 1: Free Energy of Drying for a Water Cluster Enclosed in Spherical Cavity Embedded in a Hydrophobic Material as a Function of System Size and Water/Hydrocarbon Interaction Potential[a]

potential:		$V(r)$			$V^{rep}(r)$		
ρ CH_4 #/Å^3	N_{H_2O} #	R_{sur} Å	ΔA_s kJ/mol	$\Delta A_s/A$ kJ/mol/Å^2	R_{sur} Å	ΔA_s kJ/mol	$\Delta A_s/A$ kJ/mol/Å^2
0.0233	905	18.5	369	0.086	18.4	−187	−0.04
0.0233	113	9.2	130	0.122	9.1	−44	−0.04
0.0080	113	9.2	26	0.025	9.1	−12	−0.01
potential:		$V_\infty(r)$			$V_\infty^{rep}(r)$		
ρ CH_4 #/Å^3	N_{H_2O} #	R_{surf} Å	ΔA_s kJ/mol	$\Delta A_s/A$ kJ/mol/Å^2	R_{surf} Å	ΔA_s kJ/mol	$\Delta A_s/A$ kJ/mol/Å^2
0.0233	905	18.6	223	0.051	18.6	−142	−0.03
0.0233	113	9.1	58	0.057	9.1	−27	−0.03
0.0080	113	9.1	10	0.010	9.0	−6	−0.006

[a] The area A of the water/hydrocarbon interface is calculated from R_{surf}, the position for which the oxygen density drops to half the bulk value.

The calculated values of ΔA_s are shown in Table1 for the parameters and system sizes analyzed here. In Table 1, the free-energy change per unit surface area $\Delta A_s/A$ is a normalized measure of the propensity of the water cluster to form a separated state. The surface area A is defined as the surface area of the water cluster calculated with respect to the position at which the water density is half the bulk value. The values listed for the repulsive potentials are obtained as above (eq 11) by including only the ΔA_2 term.

The water cluster does not show propensity to separate from the cavity wall in any of the models with an attractive interaction potential between the water molecules and the hydrophobic medium. Reducing the attractive part of the potential reduces the separation penalty, but it does not reverse the propensity toward the contact state. Likewise, the separated state is always favored in the models with purely repulsive wall−water interactions, and softening the repulsion does not induce a transition to a contact state.

The main driving force regulating the stability of the contact or separated states is the minimization of the water tension at the interface. The free-energy change in going from the contact to the separated state can be related to the difference in the values of the surface tension γ between the two states. The positive values of $\Delta A_s/A$ obtained with the attractive water−wall potentials indicate that in these cases the surface tension in the separated state is larger than the surface tension in the contact state. If the surface tension of the contact state is estimated from the experimental macroscopic oil/water surface tension $\Gamma_{ow} = 0.30$ kJ/mol/Å^2 [51] and the surface tension of the separated state is estimated from the experimental macroscopic vacuum−water surface tension $\Gamma_{vw} = 0.43$ kJ/mol/Å^2, we estimate $\Delta A_s/A \simeq \gamma$(separated) $- \gamma$(contact) $= 0.13$ kJ/mol/Å^2 in reasonable agreement (within a factor of 2) with the calculated values of $\Delta A_s/A$ for the attractive potentials shown in Table 1.

Conversely, the negative values of $\Delta A_s/A$ obtained with the repulsive potential indicate that under these conditions the surface tension of the separated state is smaller than the surface tension of the contact state by 0.03−0.04 kJ/mol/Å^2. The reduction of surface tension is the determinant factor in the formation of the separated state.

5. Conclusions

In this work, we have studied the structural and thermodynamic properties of a water droplet enclosed in spherical cavity embedded in a hydrophobic material. The free energy of the system was analyzed as a function of cavity size, external pressure, and water−cavity wall interaction potential to determine under which conditions a density enhancement (wetting) or a density depletion (drying) of the interface between the water droplet and the wall is favored and under which conditions the water droplet is in contact (contact state) with the wall of the cavity or is separated (separated state) from the wall by a vapor layer.

In agreement with the predictions of the analytical models of Stillinger[25] and Lum et al.,[26] the results obtained here indicate that the structure of water near an impenetrable and purely repulsive surface at standard conditions of temperature and pressure is best described as a dry, separated state. Naturally occurring hydrophobic structures in water, however, are best modeled by including a van der Waals attractive interaction between the water molecules and the nonpolar surface. It is found that the separated state is unstable if the model includes such attractive interactions, even if very weak. At ambient conditions, however, a clear density enhancement of the interface characteristic of the wet state is not observed.

The propensity toward the contact state or the separated dry state was measured quantitatively by calculating the free energy required to transform the system from the contact state to the separated dry state. The results are interpreted in terms of the tendency of the system to minimize the water−hydrophobic medium surface tension.

This work has important implications for hydration models of proteins.[24] According to the results obtained here, water molecules near hydrophobic areas of the protein surface are predicted to be in direct contact with protein atoms. Other details of the structure of proteins, such as the presence of polar and charged residues and the roughness of the protein surface, are likely to further stabilize the contact hydration state of the hydrophobic residues rather than the separated state.

The calculations presented in this paper show that adding even a weak attractive term to the repulsive water−wall interaction causes the occurrence of notable structural changes of the interface, suggesting that the structure of the hydration layer around a mesoscopic hydrophobic surface is affected by the dispersion forces between the surface and the water molecules.

Acknowledgment. This project has been supported by the National Institutes of Health Grant GM-30580 and by the High Performance Computing Project at Rutgers University. This paper has been prepared for the Festschrift in honor of Professor Bruce Berne's 60th birthday. He has pioneered the study of hydrophobic solvation using the techniques of computer simulation and we are very pleased to be able to honor him on this occasion. We thank David Chandler for his comments on the manuscript and for discussions concerning structural aspects of wetting and drying at hydrophobic interfaces.

Appendix A: Derivation of eq 1

Consider a macroscopically large volume Ω containing M ideal gas atoms and a small spherical volume of radius R impenetrable to the gas atoms and containing N molecules. The molecules interact with each other and with the ideal gas atoms. The density of the gas is assumed to be uniform. The configurational canonical partition function is

$$Q(R) = \int \mathrm{d}^M\mathbf{q}\, \mathrm{d}^N\mathbf{r}\, \mathrm{e}^{-[U_{ww}(\{\mathrm{r}\}) + U_{wq}(\{\mathbf{r}\},\{\mathbf{q}\};R)]/kT} \qquad (13)$$

where q and r are, respectively, the coordinates of the atoms of the gas and the coordinates of the molecules in the spherical volume, U_{ww} is the potential energy term due to interactions between the molecules within the spherical volume, and U_{wq} is the potential energy term due to the interactions of the molecules with the surrounding gas. We will show that eq 1 is derived from eq 13 by introducing the potential of mean force of the gas.

Integrating the q-dependent term on the right-hand side of eq 13 over the gas degrees of freedom gives

$$\begin{aligned}\int \mathrm{d}^{\mathrm{M}}\mathbf{q}\, \mathrm{e}^{-U_{wq}(\{\mathbf{r}\},\{\mathbf{q}\};R)/kT} &= \left(\int \mathrm{d}^M\mathbf{q}\right)\left\langle \mathrm{e}^{-U_{wq}(\{\mathbf{r}\},\{\mathbf{q}\};R)/kT}\right\rangle_q \\ &= \left(\Omega - \frac{4}{3}\pi R^3\right)^M \left\langle \mathrm{e}^{-U_{wq}(\{\mathbf{r}\},\{\mathbf{q}\};R)/kT}\right\rangle_q \end{aligned} \qquad (14)$$

where $\langle ... \rangle_q$ is an average over the degrees of freedom of the gas.

Retaining only the first term in the cumulant expansion we write

$$\left\langle \mathrm{e}^{-U_{wq}(\{\mathbf{r}\},\{\mathbf{q}\};R)/kT}\right\rangle_q \simeq \mathrm{e}^{-\langle U_{wq}(\{\mathbf{r}\},\{\mathbf{q}\};R)\rangle_q/kT} = \mathrm{e}^{-U_{wh}(\{\mathbf{r}\};R)/kT} \qquad (15)$$

where $U_{wh}(\{\mathbf{r}\};R)$ is the average interaction energy between the molecules and the gas introduced in eq 1. We assume here that the density of the gas is large so that the fluctuations of the U_{wq} potential energy are small, and under these conditions the cumulant approximation is valid.

We also have

$$\begin{aligned} -kT\log\left(\Omega - \frac{4}{3}\pi R^3\right)^M &= -MkT\log\left(\Omega - \frac{4}{3}\pi R^3\right) \\ &\simeq -MkT\left(\log\Omega - \frac{4\pi R^3}{\Omega}\right) \\ &= -MkT\log\Omega + P\frac{4}{3}\pi R^3 \end{aligned} \qquad (16)$$

where we have used the ideal gas equation of state $P\Omega = MkT$. The first term on the right-hand side of eq 16, $-MkT \log\Omega$, is a quantity dependent only on temperature and number of gas atoms and can be omitted; the second term is

$$P\frac{4}{3}\pi R^3 = PV(R) \tag{17}$$

where $V(R)$ is the volume of the spherical volume.

The potential of mean force of the gas is therefore

$$\int \mathrm{d}^M\mathbf{q}\, \mathrm{e}^{-U_{\mathrm{wq}}(\{\mathbf{r}\},\{\mathbf{q}\};R)/kT} \simeq \mathrm{e}^{-[U_{\mathrm{wh}}(\{\mathbf{r}\};R) + PV(R)]/kT} \tag{18}$$

eq 1 is recovered by inserting eq 18 into eq 1.

Appendix B: Equivalence with Gibbs Ensemble

Figure 5 shows the Helmoltz free energy as a function of cavity radius at a series of pressures P. In this section, we show that in the thermodynamic limit at the minimum of each of the curves the value of the Helmoltz free energy equals the value of the Gibbs free energy of the water droplet at the external pressure P. The derivation is based on the standard procedure to demonstrate the equivalence of the Gibbs and Helmoltz ensembles (see, for example, ref 52).

The isobaric partition function of the water droplet in the cavity is

$$\Delta(P) = \int \mathrm{d}V\, \mathrm{e}^{-[PV + F(V)]/kT} \tag{19}$$

where $F(V)$ is the Helmoltz free energy of the water droplet in the cavity, defined by eq 3, evaluated at the radius $R = (3\mathrm{V}/4\pi)^{1/3}$. By replacing the integrand of eq 19 by a Gaussian centered at the maximum, V^*, of the integrand, we obtain

$$\Delta(P) \simeq \mathrm{e}^{-[PV^* + F(V^*)]}\sqrt{\frac{\pi kT\kappa_{\mathrm{T}}V^*}{2}} \tag{20}$$

where

$$\kappa_{\mathrm{T}} = -\frac{1}{V^*}\left(\frac{\partial V}{\partial P}\right)_{T,V=V^*} = \frac{1}{V^*}\left[\left(\frac{\partial^2 F(V)}{\partial V^2}\right)_{T,V=V^*}\right]^{-1} \tag{21}$$

is the isothermal compressibility of the droplet and V^* is the volume at the maximum of the volume distribution function of the cavity $\exp\{-\beta[PV + F(V)]\}$ or, equivalently, the volume corresponding to the minimum of $PV + F(V)$. At $V = V^*$, we have

$$P = -\frac{\partial F(V)}{\partial V} \tag{22}$$

which corresponds to the equalization between the internal pressure of the droplet and the external pressure, a condition necessary for the mechanical equilibrium of the cavity. In conclusion, $R^* = (3V^*/4\pi)^{1/3}$; the minimum of the function $A(R) = F(R) + PV(R)$, corresponds to the equilibrium cavity size in the constant pressure ensemble.

From eq 20, the Gibbs free energy is

$$G(P) = -kT \log \Delta(P) \simeq F(V^*) + PV^* - \frac{kT}{2}\log\frac{\pi kT\kappa_{\mathrm{T}}V^*}{2} \tag{23}$$

In the thermodynamic limit (number of molecules $N \rightarrow \infty$), the last term on the right-hand side of eq 23 is negligible with respect to the $F(V^*) + PV^*$ and

$$G(P) = F(V^*) + PV^* \tag{24}$$

Thus, the minimum value of the thermodynamic potential $A(R) = F(R) + PV(R)$ is, in the thermodynamic limit, the Gibbs free energy of the water droplet in the cavity at the external pressure P.

References and Notes

(1) Blokzijl, W.; Engberts, J. B. F. N. *Angew. Chem., Int. Ed. Engl.* **1993**, *32*, 1545−1579.
(2) .Pratt, L. R.; Chandler, D. *J. Chem. Phys.* **1977**, *67*(8), 3683−3704.
(3) .Pratt, L. R.; Chandler, D. *J. Chem. Phys.* **1980**, *73*(7), 3434−41.
(4) .Pangali, C.; Rao, M.; Berne, B. J. *J. Chem. Phys.* **1979**, *71*, 2975−2981.
(5) Pangali, C.; Rao, M.; Berne, B. J. *J. Chem. Phys.* **1979**, *71*, 2982−2990.
(6) Watanabe, K.; Andersen, H. C. *J. Phys. Chem.* **1986**, *90*, 795−802.
(7) .Tobias, D. J.; Brooks, C. L., III *Chem. Phys. Lett.* **1987**, *142*, 472−476.
(8) Ravishanker, G.; Mezei, M.; Beveridge, D. L. *Faraday Symp. Chem. Soc.* **1982**, *17*, 79−91.
(9) Lee, B. *Biopolymers* **1985**, *24*, 813−23.
(10) Wallqvist, A. *J. Phys. Chem.* **1991**, *95*, 8921−27.
(11) Guillot, B.; Guissani, Y.; Bratos, S. *J. Chem. Phys.* **1991**, *95*, 3643−3648.
(12) Smith, D. E.; Zhang, L.; Haymet, A. D. J. *J. Am. Chem. Soc.* **1992**, *114*, 5875−5876.
(13) Smith, P. E.; Brunne, R.; Mark, A. E.; van Gunsteren, W. F. *J. Phys. Chem.* **1993**, *97*, 2009−2014.
(14) .van Belle, D.; Wodak, S. J. *J. Am. Chem. Soc.* **1993**, *115*, 647−652.
(15) Dang, L. X. *J. Chem. Phys.* **1994**, *100*, 9032.
(16) Hummer, G.; Garde, S.; Garcıa, A. E.; Pohorille, A.; Pratt, L. R. *Proc. Natl. Acad. Sci. U.S.A.* **1996**, *93*, 8951−8955.
(17) Hydration Processes in Biological and Macromolecular Systems. *Faraday Discus.* **1996**, *103*.
(18) Gallicchio, E.; Kubo, M.; Levy, R. M. *J. Phys. Chem. B* **2000**, *104*, 6271−6285.
(19) Rowlinson, J. S.; Widom, B.; *Molecular Theory of Capillarity*. Oxford University Press: Oxford, 1982.
(20) Truskett, T. M.; Debenedetti, P. G.; Torquato, S. *J. Chem. Phys.* **2001**, *114*, 2401.
(21) Weeks, J. D.; Selinger, R. L. B.; Broughton, J. Q. *Phys. Rev. Lett.* **1995**, *75*, 2694.
(22) Kauzmann, W. *Adv. Protein Chem.* **1959**, *14*, 1−63.
(23) Wood, R. H.; Thompson, P. T. *Proc. Natl. Acad. Sci. U.S.A.* **1990**, *87*, 946−949.
(24) Huang, D. M.; Chandler, D. *Proc. Natl. Acad. Sci. U.S.A.* **2000**, *97*, 8324−8327.
(25) Stillinger, F. H. *J. Sol. Chem.* **1973**, *2*, 141−158.
(26) Lum, K.; Chandler, D.; Weeks, J. D. *J. Phys. Chem. B* **1999**, *103*, 4570−4577.
(27) Pashley, R. M.; McGuiggan, P. M.; Ninham, B. W. *Science* **1985**, *229*, 1088.
(28) Christenson, H. K.; Claesson, P. M. *Science* **1988**, *239*, 390.
(29) Jönsson, B. *Chem. Phys. Lett.* **1981**, *82*, 520−525.
(30) Marchesi, M. *Chem. Phys. Lett.* **1983**, *97*, 224−230.
(31) Lee, C. Y.; McCammon, J. A.; Rossky. P. J. *J. Chem. Phys.* **1984**, *80*, 4448−4455.
(32) Wallqvist, A. *Chem. Phys. Lett.* **1990**, *165*, 437−442.
(33) Wallqvist, A.; Berne, B. J. *J. Phys. Chem.* **1995**, *99*, 2885−2892.
(34) Wallqvist, A.; Berne, B. J. *J. Phys. Chem.* **1995**, *99*, 2893−2899.
(35) Hummer, G.; Garde. S. *Phys. Rev. Lett.* **1998**, *80*, 4193−4196.
(36) Franks, F. Ed.; *Water, A Comprehensive Treatise*; Plenum: New York, 1972−1982; Vols 1−7.
(37) Tanford, C. *The hydrophobic effect: formation of micelles and biological membranes*; Wiley: New York, 1973.
(38) Dill, K. A. *Biochemistry* **1990**, *29*, 7133−7155.
(39) Privalov, P. L.; Makhatadze. G. I. *J. Mol. Biol.* **1993**, *232*, 660−679.
(40) Honig, B.; Yang, A.-S. *Adv. Protein Chem.* **1995**, *46*, 27−58.
(41) Sturtevant, J. M. *Proc. Natl. Acad. Sci. U.S.A.* **1977**, *74*, 2236−2240.
(42) Williams, D. H.; Searle, M. S.; Mackay, J. P.; Gerhard, U.; Maplestone, R. A. *Proc. Natl. Acad. Sci. U.S.A.* **1993**, *90*, 1172−78.
(43) Froloff, N.; Windemuth, A.; Honig, B. *Protein Sci.* **1997**, *6*, 1293−1301.
(44) Bolhuis, P. G.; Chandler, D. *J. Chem. Phys.* **2000**, *113*(18), 8154.

(45) Berendsen, H. J. C.; Grigera, J. R.; Straatsma, T. P. *J. Phys. Chem.* **1987**, *91*, 6269−6271.
(46) Wallqvist, A.; Berne, B. J. *Chem. Phys. Lett.* **1988**, *145*, 26−32.
(47) Wallqvist, A. *Chem. Phys.* **1990**, *148*, 439−449.
(48) Weeks, J. D.; Chandler, D.; Andersen, H. C. *J. Chem. Phys.* **1971**, *54*(12), 5237−47.
(49) Andersen, H. C. *J. Comput. Phys.* **1983**, *52*, 24.
(50) Swope, W. C.; Andersen, H. C.; Berens, P. H.; Wilson, K. R. *J. Chem. Phys.* **1982**, *76*, 637−649.
(51) Tanford, C. H. *Proc. Natl. Acad. Sci.* **1979**, *76*, 4175−4176.
(52) Hill, T. L. *Statistical Mechanics: Principles and Selected Applications*; McGraw-Hill: New York, 1956.